Research Article

Unveiling optical rogue wave behavior with temporally localized structures in Brillouin random fiber laser comb

Yuxi Pang,[a,b] Qiang Ji,[a,b] Shaonian Ma,[a,b] Xian Zhao,[a,b] Zengguang Qin,[b,c] Zhaojun Liu,[b,c] Ping Lu,[d] Xiaoyi Bao,[e] and Yanping Xu[a,b,*]

[a]Shandong University, Center for Optics Research and Engineering, Qingdao, China
[b]Shandong University, Key Laboratory of Laser and Infrared System of the Ministry of Education, Qingdao, China
[c]Shandong University, School of Information Science and Engineering, Qingdao, China
[d]National Research Council Canada, Ottawa, Canada
[e]University of Ottawa, Physics Department, Ottawa, Canada

Abstract. The optical rogue wave (RW), known as a short-lived extraordinarily high amplitude dynamics phenomenon with small appearing probabilities, plays an important role in revealing and understanding the fundamental physics of nonlinear wave propagations in optical systems. The random fiber laser (RFL), featured with cavity-free and "modeless" structure, has opened up new avenues for fundamental physics research and potential practical applications combining nonlinear optics and laser physics. Here, the extreme event of optical RW induced by noise-driven modulation instability that interacts with the cascaded stimulated Brillouin scattering, the quasi-phase-matched four-wave mixing as well as the random mode resonance process is observed in a Brillouin random fiber laser comb (BRFLC). Temporal and statistical characteristics of the RWs concerning their emergence and evolution are experimentally explored and analyzed. Specifically, temporally localized structures with high intensities including chair-like pulses with a sharp leading edge followed by a trailing plateau appear frequently in the BRFLC output, which can evolve to chair-like RW pulses with adjustable pulse duration and amplitude under controlled conditions. This investigation provides a deep insight into the extreme event of RWs and paves the way for RW manipulation for its generation and elimination in RFLs through adapted laser configuration.

Keywords: optical rogue wave; modulation instability; random fiber laser; cascaded stimulated Brillouin scattering; four-wave mixing; temporally localized structure.

1 Introduction

Rogue waves (RWs), derived from oceanography,[1] were first investigated in the framework of hydrodynamics,[2] referring to the rarely encountered waves with extremely high amplitude larger than the expected ordinary wave amplitude on the surface of the ocean. Recently, similar phenomena have been observed in many other fields of science, especially the so-called optical RWs in the field of laser physics, which is initially proposed and experimentally observed during the process of supercontinuum generation.[3] The optical RWs, referring to intensity fluctuations of light with amplitude drastically larger than the average value, were then successively observed and recorded in various nonlinear optical systems, including supercontinuum generation systems,[4] Raman fiber amplifier systems,[5] semiconductor lasers,[6] Ti:sapphire lasers,[7] solid-state lasers,[8] microcavity lasers,[9] and random lasers.[10] In fact, the generation of optical RWs relies heavily on various nonlinear effects in optical systems. The one-dimensional waveguide of optical fiber is of great value in the investigation of optical nonlinear effects. It exhibits a relatively

*Address all correspondence to Yanping Xu, yanpingxu@sdu.edu.cn

low threshold of nonlinear effects due to its light-wave confinement ability that allows the light wave to propagate with relatively high field strength. Meanwhile, it also maintains a long coherence transmission distance for nonlinear interaction thanks to its low optical loss. Thus, the optical RWs have been studied in various optical fiber systems, including Raman fiber amplifiers,[11] optical filamentation,[12] Raman fiber lasers,[13] ultrafast fiber lasers,[14] and random fiber lasers (RFLs).[15] Among them, RFLs, as a unique platform with rich physical processes and nonlinear optical effects, have not been fully investigated in the exploration of optical RWs and their physical mechanisms.

Recently, RFLs have received a lot of attention due to their attractive features like low cost, simplicity of fabrication, and modeless lasing output. To date, RFLs based on a variety of gain mechanisms including rare-earth ion-doped fiber amplifiers,[16] stimulated Brillouin scattering (SBS),[17] stimulated Raman scattering,[18,19] and semiconductor optical amplifiers[20] have been reported. By employing regulating and control technologies combined with different gain mechanisms, performances of the reported RFLs have been well improved in many aspects, especially in their lower threshold,[21] higher output power,[22] wavelength tunability,[23] higher coherence,[24] narrower linewidth,[25] lower noise,[26] and more stabilized output power,[27] which enables a wide range of applications for RFLs in optical measurement,[28] microwave photonics,[29] optical fiber communication,[30] optical fiber sensing,[31] laser imaging,[32] and other fields.[30,33] Among the above-mentioned RFLs based on different gain mechanisms, the Brillouin random fiber laser (BRFL) stands out by right of its excellent properties, such as the low threshold in long single-mode fiber (SMF), narrow gain bandwidth (~30 to 40 MHz in standard SMF), high amplification factor, and inhomogeneous broadening gain spectrum. In particular, the ease of triggering the cascaded SBS effect in optical fibers makes RFL based on SBS an excellent candidate for achieving a random laser comb with fixed wavelength intervals among all the RFLs. Indeed, the Brillouin random fiber laser comb (BRFLC) has attracted a great deal of attention and has been heavily investigated.[34,35] It is an all-fiber compact source with multiplexed narrow linewidth wavelength components with fixed spectral intervals, which can be achieved without introducing extra devices for frequency shifting or multichannel filtering. In recent years, several investigations[36,37] on BRFLC have been reported, which mainly focus on the improvement in the degree of linear polarization of the lasing output, the number of lasing orders, the optical signal-to-noise ratio (OSNR) of each lasing line, the peak power discrepancy, and the wavelength tunability. With their unprecedented lasing properties, BRFLCs have shown great potential for applications in the fields of wavelength-division-multiplexing communication systems,[38] sensor networks,[39] and precision spectroscopy.[29] However, there exist concerns that the requirements for high pump power and long Brillouin gain fiber (usually with high nonlinearity coefficients for realizing a highly efficient BRFLC) would inevitably induce undesired complex interactions between various physical processes and nonlinear optical effects including the modulation instability (MI), the cascaded SBS process, and the four-wave mixing (FWM) process, which would be further disturbed by the random mode resonances specifically present in the open cavity of RFLs, leading to unstable operation characterized by random emission of giant transient pulses, i.e., optical RWs. This may cause irreversible damage to the laser system itself, severely limiting the performance

and applicability of BRFLCs. Up to now, optical RWs have been observed in random lasing-assisted cascaded supercontinuum generation,[4] Yb-doped RFLs,[40] and Raman random fiber lasers,[15] in which statistical dynamics of the generated optical RWs are investigated and analyzed. However, compared with the above-mentioned RFL systems based on stimulated Raman scattering or rare-earth-doped fiber amplification, the BRFLC is a different laser comb system involving a variety of physical processes, including the modulation instability process, the cascaded SBS process, the quasi-phase-matched FWM process, as well as the random mode resonances, which would definitely exhibit richer statistical temporal dynamics and RW behaviors that need to be thoroughly studied. Indeed, optical RW behavior in BRFLC and its underlying links with the physical processes have not been investigated and presented in detail. Studies on the generation and evolution of RWs in BRFLC are crucial for revealing and understanding the physical mechanisms of the lasing behaviors, which also provides instructive guidance for the design and performance optimization of BRFLCs.

In this paper, extreme events of optical RWs are observed with temporally localized structures in a typical BRFLC. The generation of RWs is attributed to the noise-driven MI that interacts with the cascaded SBS, the quasi-phase-matched FWM, as well as the random mode resonance process. In this complex nonlinear interaction process, the noise-driven MI is enhanced to the induced MI process by the cascaded SBS process and the quasi-phase-matched FWM process by providing the new frequency components as the seed. Consequently, the noise-induced optical perturbations are significantly amplified by the enhanced MI, which thus imposes unstable temporal modulations on the resonant Stokes/anti-Stokes lights, giving rise to the extreme events of the optical RWs. The temporal and statistical characteristics of the RWs' behavior regarding its emergence and evolutions are experimentally explored and analyzed. In addition, temporally localized structures of chair-like pulses appear frequently in the output of BRFLC, with a sharp leading edge followed by a trailing plateau, which can evolve into chair-like RW pulses with adjustable pulse rate, duration, and amplitude under controlled laser parameters, thus proving the potential for manipulating RWs in the BRFLC system.

2 Experiments

2.1 Experimental Configuration

A rather typical setup has been adapted to investigate and characterize the optical RW behavior in the BRFLC, as shown in Fig. 1. As illustrated, the BRFLC consists of a half-open main cavity responsible for random lasing oscillation and a subcavity that amplifies and re-injects the generated Brillouin Stokes/anti-Stokes lights into the main cavity. A 1550-nm semiconductor laser (LIGHTPROMOTECH, NLLD 0175-3-34-2) is used as the pump light source, with a maximum output power of 10-dBm and a linewidth of ~15 kHz. After passing through several optical devices, light from the pump laser enters the main cavity and is launched into a 390-m-long highly nonlinear fiber (HNLF). The first isolator (ISO1) added along the path of the pump light is to prevent any potential reflected light to protect the pump laser. The erbium-doped fiber amplifier (EDFA) and the second variable optical attenuator (VOA2) are used cooperatively to precisely adjust the pump power. Subsequently, the first polarization controller (PC1) is utilized to regulate the
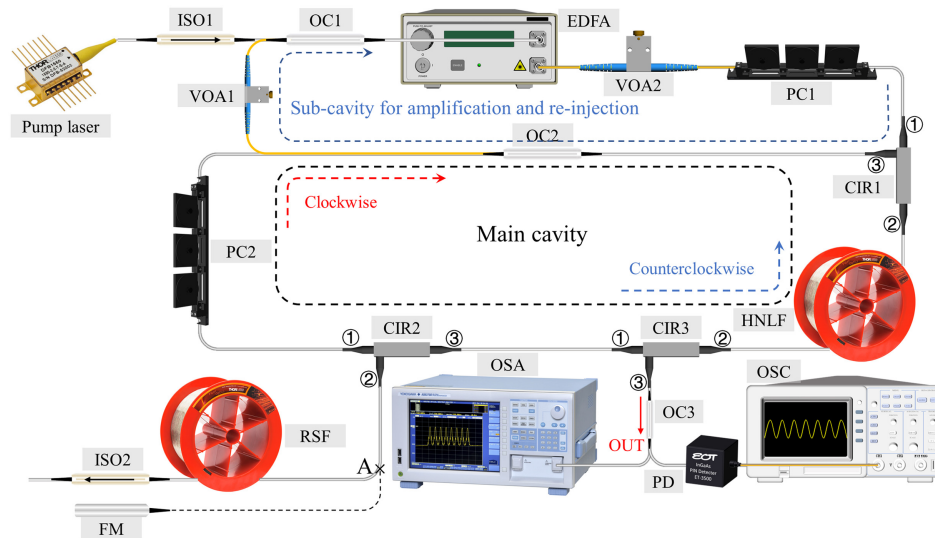
Fig. 1 Experimental setup of the BRFLC. (ISO, isolator; OC, optical coupler; EDFA, erbium-doped fiber amplifier; VOA, variable optical attenuator; PC, polarization controller; CIR, circulator; HNLF, highly nonlinear fiber; RSF: Rayleigh scattering fiber; OSA, optical spectrum analyzer; PD, photodetector; OSC, oscilloscope; FM, fiber mirror.

polarization states of the pump light and the Brillouin Stokes/ anti-Stokes lights that are coupled back through the subcavity, ensuring optimal SBS efficiency within the main cavity. Initially, with weak pump power, the Stokes light is generated by the spontaneous Brillouin scattering (SpBS) process in the main cavity. The generated Stokes light propagating in the opposite direction of the pump light has a frequency downshift of approximately 10 GHz compared to the pump light due to the Doppler shift.[41] When the pump power is increased to the level that reaches the excitation threshold of the SBS process, the initially produced Stokes light through SpBS is significantly amplified by the SBS process with an extension in its coherent time.[42] The amplified counterpropagating Stokes light enters the first circulator (CIR1) through Port 2 and exits from Port 3, which is then equally divided by the second optical coupler (OC2) into two parts, with one part entering the subcavity and the other part continuing to propagate in the main cavity. Then, the latter part of the Stokes light enters a 5-km-long SMF, i.e., the Rayleigh scattering fiber (RSF), through CIR2 after polarization adjustment by PC2. ISO2 is connected at the far end of the RSF to avoid Fresnel reflection at the end face. Within the RSF, the Stokes light is randomly scattered along the fiber owing to the Rayleigh scattering effect and a small fraction of the scattered Stokes light propagates backward into the main cavity. Since the SBS process contributes high coherence to the generated Stokes light, the multiply backscattered Stokes lights along the RSF interfere constructively, leading to the generation of coherent random resonant spikes when the backscattered Stokes light re-enters the main cavity and rejoins the SBS process within the HNLF for lasing resonances. The Stokes light is repeatedly amplified each time it circulates in the main cavity, which results in a rapid increase in its power. Once the gradually accumulated effective Brillouin gain of Stokes light is sufficiently high to overcome the total loss in the entire cavity, the Stokes light starts to resonate in the main cavity. Part of the resonant Stokes light is extracted from the main cavity and directed into the subcavity through OC2. Within

the subcavity, the power of the Stokes light is adjusted using VOA1, which is then combined with the pump light through OC1. The mixed light is further amplified by the EDFA and subsequently launched into the main cavity to generate higher-order Stokes lights through the cascaded SBS process. The newly generated higher-order Stokes light can be resonated within the main cavity as long as the accumulated Brillouin gain is sufficiently high to overcome the total loss in the entire cavity. Part of the resonant higher-order Stokes light is then guided into the subcavity and mixed with the pump light, which is injected back into the main cavity once again to act as the Brillouin pump for generating the subsequent-order Stokes light. These cascaded SBS resonances in the main cavity eventually lead to the buildup of the random lasing comb with multiple wavelength components. It is worth mentioning that the FWM process is also involved in the operation of the above-mentioned BRFLC, which boosts the power of existing Stokes lights and facilitates the generation of higher-order Stokes lights and anti-Stokes lights. This is achieved by appropriately adjusting the power and polarization of the pump light to satisfy the quasi-phase-matched condition for the clockwise-propagating multi-order Stokes/anti-Stokes light and the pump light. Note that the clockwise-propagating Stokes/anti-Stokes lights in the main cavity would also be backscattered through Raleigh scattering along the HNLF. The backscattered counterclockwise-propagating Stokes/anti-Stokes lights are then re-injected in the main cavity through the subcavity, which act as the feedback for the FWM process among clockwise-propagating Stokes/ anti-Stokes pump lights. During each round trip of these Stokes/anti-Stokes lights in the main cavity, the gain is provided by the cascaded SBS process, the FWM process, and the EDFA in the subcavity. Once the accumulated gain overcomes the total optical loss, the Stokes/anti-Stokes lights would start to resonate in both clockwise and counterclockwise directions, which further facilitates the realization of the random lasing comb. The generated random lasing comb is eventually emitted at Port 3 of CIR3, which is then filtered using a tunable optical filter so that

Stokes/anti-Stokes light of a specific order can be selected for analysis concerning their temporal and spectral characteristics using an oscilloscope (OSC) and an optical spectrum analyzer (OSA). In the experiment, the length of the RSF is altered to evaluate the influence of varied random distributed feedback on the optical RWs' behavior. In addition, a fiber mirror (FM) is also utilized to replace the RSF for comparing optical RWs' behaviors associated with fixed-point reflection feedback and random distributed feedback.

2.2 Physical Principles

The working principle of the BRFLC is illustrated in Fig. 2. As mentioned in the section above, in the dual-cavity configuration, multi-order Stokes lights and anti-Stokes lights generated through the cascaded SBS process circulate in both clockwise and counterclockwise directions, as shown in Fig. 2(a). The Stokes lights are able to resonate with the gain provided by the cascaded SBS process and the FWM process as well as random distributed feedback from the RSF and the HNLF. In contrast, the anti-Stokes lights resonate with little gain from the cascaded SBS process but the gain is provided by the FWM process. Note that in the BRFLC, the FWM process in the clockwise direction is more efficient owing to the sufficiently high pump power and the corresponding higher parametric gain. As shown in Fig. 2(b), the FWM process occurs among the pump light and Stokes/anti-Stokes lights, which act as the pump or signal light (marked by the gray solid circles) to give rise to the idler lights (marked by the white solid circles). In fact, all the pump lights, Stokes lights in the cascaded SBS process, and the newly generated anti-Stokes lights during the FWM process can act as the pump light or signal light to participate in the FWM to produce other idler lights, as illustrated by the six

FWM processes with different combinations of pump, signal, and idler lights in Fig. 2(b). Owing to the consistent frequency interval between Stokes lights of neighboring orders determined by the nature of the cascaded SBS process, the frequency interval between the idler lights created in the FWM process is a multiple of the original frequency interval. With the cooperative interaction between the cascaded SBS process and the FWM process, a large number of higher-order Stokes and anti-Stokes lights can be effectively generated and enhanced in the main cavity, facilitating the random laser comb generation with multi-order Stokes and anti-Stokes lights.

It is worth noting that how well the phase-matching condition of the FWM process is satisfied is crucial in determining the efficiency and the parametric gain of this nonlinear process. The phase-matching condition can be regarded to be met for the FWM process when the phase mismatch factor κ ($\kappa = \Delta\beta + 2\gamma P$) is equal to zero, where γP is the nonlinear phase shift caused by self-phase modulation and cross-phase modulation, γ represents the nonlinear coefficient of fiber, and P denotes the pump power. $\Delta\beta = -2\pi c[D(\lambda_p - \lambda_s)^2]/\lambda_0^2$ is the linear phase shift due to the different propagation constants of the lights and is negative only in the anomalous dispersion region, where c is the speed of light in vacuum, D is dispersion, λ_p and λ_s are the wavelengths of pump and signal light, respectively, and λ_0 is the zero-dispersion wavelength of the optical fiber. $\Delta\beta$ can offset part of the positive value of γP and make κ equal to zero to meet the phase-matching condition of FWM. However, this rigorous phase-matching condition is difficult to achieve in most cases where the FWM process occurs with quasi-phase-matching condition (κ close to zero but not equal to zero), in which the efficiency or the parametric gain of the FWM is not optimum. Therefore, the FWM process can effectively take place for light waves with a certain bandwidth,
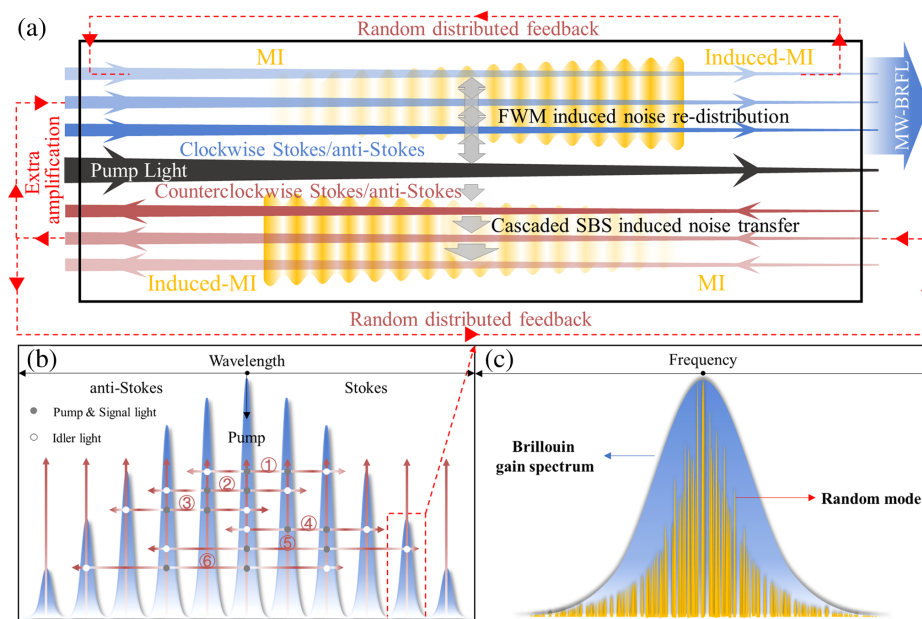
Fig. 2 Schematic diagram of (a) the operation principle of the BRFLC and the interplay among the noise-driven MI, the cascaded SBS, and the quasi-phase-matched FWM process; (b) the cascaded SBS process and the quasi-phase-matched FWM process occurring among multiple Stokes and anti-Stokes lines; and (c) random mode distribution within the Brillouin gain spectrum for a certain Stokes/anti-Stokes line.

as long as the phase mismatch factor κ is close to zero for any spectral component within the associated light waves. The parametric gain coefficient of the FWM process is expressed as

$$\begin{cases} g = \sqrt{(\gamma P_0 r)^2 - (\kappa/2)^2} \\ r = 2\sqrt{P_1 P_2}/P_0 \\ P_0 = P_1 + P_2, \end{cases} \quad (1)$$

in which P_1 and P_2 are the power of incident lights with frequencies f_i and f_j, respectively, used for generating a light wave with a new frequency (f_k). To characterize the quasi-phase-matched FWM process in the BRFLC, the relationship between the parametric gain coefficient of FWM and the linear phase shift $\Delta\beta$, as well as the order-difference of interacting multi-order Stokes and anti-Stokes light, respectively, was analyzed using Eq. (1). Simulation results were then obtained and presented in Fig. 3. In Fig. 3(a), it can be observed that the parametric gain of FWM exists within a range of $-4\gamma P < \Delta\beta < 0$ (equivalent to $-2\gamma P < \kappa < 2\gamma P$), with the maximum gain value found at $\Delta\beta = -2\gamma P$ ($\kappa = 0$). Higher sum-power provides a larger parametric gain of FWM in a broader range of linear dispersion shifts. To investigate quasi-phase-matched FWM process occurring among multi-order Stokes and anti-Stokes lights in the BRFLC, the parametric gain coefficient of FWM for order-difference up to 60 for both Stokes and anti-Stokes lights is simulated using Eq. (1) at different sum powers. The parametric gain coefficient of FWM as a function of the order-difference between two Stokes/anti-Stokes lights was simulated; the findings are depicted in Fig. 3(b). Here, positive and negative order-differences represent $f_i > f_j$ and $f_i < f_j$, respectively. It can be observed from Fig. 3(b) that, similar to the results obtained in Fig. 3(a), a maximum parametric gain occurs at a specific order-difference and the FWM effect is cut off at a larger order-difference. All the combinations of Stokes/anti-Stokes lights with the order-difference less than the cutoff value can participate in the FWM process under the quasi-phase-matched condition to obtain the parametric gain. Additionally, the overall profile of the FWM gain coefficient also increases with the sum power of the two signal lights involved in the process. And the order-difference for both the maximum parametric

gain and the gain cutoff shifts to larger values with the sum power. This implies that amplifying the sum power of interacting signal lights can enhance the parametric gain of FWM among Stokes/anti-Stokes lights with a large order-difference for generating or amplifying new Stokes/anti-Stokes lines.

Since the zero-dispersion wavelength of the HNLF is located around 1521 nm, the pump wavelength is set as 1550 nm in the experiment so that the pump light can be boosted to satisfy the quasi-phase-matching condition for the FWM process. To show that the quasi-phase-matching condition is satisfied in the proposed system, the phase mismatch factor κ is calculated with the following parameters of $c = 3 \times 10^8$ m·s^{-1}, $D = 0.5753183$ ps·nm^{-1}·km^{-1} (@ 1550 nm), $\lambda_p = 1550$ nm, $\lambda_s = 1551.14$ nm (@ 15th-order Stokes light), $\lambda_0 = 1521.78962$ nm, $\gamma = 10$ W^{-1}·km^{-1}, and $P = 50$ mW. The result shows that the calculated value for κ is 0.00039142 m^{-1}, which is close to zero. It is worth noting that κ maintains low values that are close to zero in the range from $\sim1.589 \times 10^{-8}$ to ~0.001997 for cases in which there is one order-difference between the pump light and the signal light when λ_p and P are varied in the ranges of $1500 - 1560$ nm and $0 - 100$ mW, respectively, indicating that the FWM process would be effectively triggered and operated in the current system.

In the BRFLC, the 5-km-long SMF provides random distributed feedback via the Rayleigh scattering effect at multiple scattering points with nonuniform refractive index distribution and random scattering coefficients and locations, which contributes to numerous densely spaced longitudinal modes with random spacing in the resonant cavity. As shown in Fig. 2(c), the densely spaced random modes located within the Brillouin gain bandwidth intensively compete for the limited Brillouin gain, leading to mode hopping and multimode resonance phenomena within the resonant cavity. This introduces severe random frequency and intensity fluctuations to the resonant light. In addition, the random distributed Rayleigh scattering points introduce stochastic delays for the resonant modes with different mode spacing. This significantly decreases the phase correlation between the random modes and further enhances the intensity fluctuations of the resonant light. Consequently, the induced random phase variations of the scattered Stokes light would result in random changes in both the frequency and amplitude of the coherent random spikes formed by the constructive
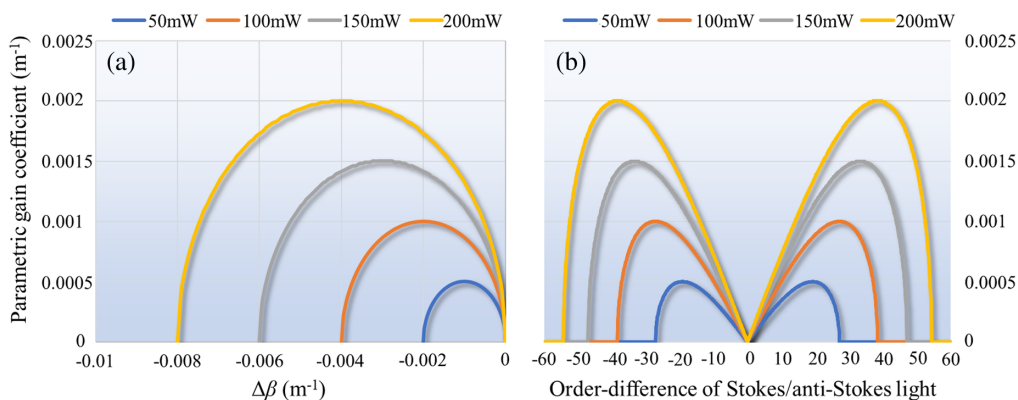
Fig. 3 Simulations of parametric gain coefficient versus (a) linear phase shift $\Delta\beta$ and (b) order-difference up to 60 for both Stokes and anti-Stokes lights at different sum powers of 50, 100, 150, and 200 mW of two interacting Stokes/anti-Stokes lights as the pump and signal lights in the quasi-phase-matched FWM process.

coherence among the random modes. Therefore, the random mode hopping and intensive multimode resonance within the Brillouin gain bandwidth induced by a large number of densely spaced random longitudinal modes lead to highly decorrelated and chaotic dynamics in the resonant light.

MI is a general nonlinear optical process occurring during the light-wave propagation in nonlinear media in the anomalous dispersion regime, which can lead to the exponential growth of co-propagation noise due to the interplay between the nonlinear and dispersion effects.[43] There are three main sources of noise involved in the MI process during the operation of the BRFLC. First, as the BRFLC is initially driven by the SBS generation process, in which the SBS process starts from the nonlinear amplification of the thermal noise along the fiber, it inevitably inherits the SBS-induced instabilities arising from the intrinsic noise-seeded process and exhibits self-pulsing instabilities. In the cascaded SBS process, the power, phase, and polarization of each higher-order Stokes light are highly related to the state of the adjacent lower-order Stokes light due to the intrinsic phase-matching requirement. Therefore, a large amount of noise originated either from the thermal noise or the random mode resonances in each-order Stokes light is transferred order by order to the higher-order Stokes lights in the cascaded SBS process, which is illustrated by the red bars representing the resonant multi-order Stokes/anti-Stokes lights and the gray one-way arrows denoting cascaded SBS-induced noise transfer in Fig. 2(a). As the cascaded SBS process proceeds from low-order to high-order Stokes light, the Stokes light of higher order will accumulate more noises generated and transferred from the low-order Stokes lights and therefore exhibit a more severe instability. The second one is the random mode resonance process, in which the densely spaced randomly distributed longitudinal modes within the Brillouin gain bandwidth competing for the finite Brillouin gain result in severe mode hopping and multimode resonance and thus introduce significant instabilities in the resonant Stokes and anti-Stokes lights. The third one is the quasi-phase-matched FWM process, which covers the pump light and almost all the Stokes/anti-Stokes lights, the noises and instabilities due to the intrinsic noise-seeded SBS process. and the random mode resonance present in the resonant Stokes lights generated through the cascaded SBS process would be transferred and redistributed among all the associated Stokes/anti-Stokes lights, especially the newly generated idler lights in the quasi-phase-matched FWM process. In addition, the resonant Stokes/anti-Stokes lines are also influenced by the noises induced by external noise perturbations and active optical devices in the laser system, including pump noise, temperature disturbance-induced cavity-length modulation,[44] and EDFA-introduced amplified spontaneous emission.[45] Moreover, in the SBS process, the excitation of the electrostriction process introduces additional random pressure and acoustic vibration that are superimposed with the existing acoustic waves and interact with the pump and Stokes light. This leads to additional random phase fluctuations in the generated Stokes lights.[46] These noises would also be spread unequally among all generated Stokes/anti-Stokes light via the cascaded SBS process and the quasi-phase-matched FWM process, leading to a more pronounced level of instabilities and disorders in the output of the random laser comb. In the BRFLC, the noise-driven MI process interacts with the cascaded SBS, the quasi-phase-matched FWM, and the random mode resonance process, which in turn significantly amplifies the noise-induced optical perturbations and thus

imposes unstable temporal modulations on the resonant Stokes/anti-Stokes lights, transforming the continuous laser output to a self-pulsing one. More importantly, the new spectral components generated through the cascaded SBS and the quasi-phase-matched FWM process act as the seed to trigger the induced MI, which further enhances the unstable temporal modulations on the resonant Stokes and anti-Stokes lights as represented by the yellow regions in Fig. 2(a), leading to the emergence of giant transient pulses, i.e., the RWs. Considering the local noises induced by the random mode resonance and the SBS process in each order of the Stokes/anti-Stokes line as well as the noise transfer and redistribution provided by the cascaded SBS and the quasi-phase-matched FWM process, the comprehensive MI-induced unstable temporal modulation imposed in each Stokes/anti-Stokes line is expected to follow an evolution trajectory with the order number.

3 Results and Discussion

In the experiment, the number of the generated Stokes/anti-Stokes lines in the output of BRFLC grows with the pump power, and up to 21 orders of Stokes lines and 18 orders of anti-Stokes lines are achieved when the pump power is amplified to 810 mW, as shown by the optical spectra of the BRFLC output in Figs. 4(a) and 4(b). It is seen that the generated Stokes/anti-Stokes light exhibits a high OSNR (maximum of ~44.074 dB) thanks to the high pumping power, high Brillouin gain coefficient provided by the HNLF, and high parametric gain provided by the FWM process. Figures 4(c) and 4(d) show the calculated power spectra of first-order Stokes light of the Brillouin fiber laser comb with the random distributed feedback provided by the 5-km-long SMF and mirror feedback provided by the FM. It is seen from Fig. 4(c) that there are no peaks arising from beatings between cavity modes, verifying the modeless operation of the BRFLC. In contrast, periodic spikes with constant frequency intervals are observed in the power spectrum of the first-order Stokes light in the case of mirror feedback, as shown in Fig. 4(d). The frequency interval of the adjacent spikes is ~534 kHz, which agrees well with the cavity length of ~390 m according to the equation $\Delta v = c/nL$.

To characterize the temporal dynamics of the laser output, the first eight orders of Stokes lines and the first eight orders of anti-Stokes lines with the highest OSNRs and intensities as well as the residual pump light are individually filtered out by a tunable bandpass filter (Alnair, BVF-300CL-SM-FA). Then the temporal intensity traces of the filtered Stokes, anti-Stokes, and residual pump lights are acquired by a high-speed photodetector (EOT, ET-3500FEXT/APC) with a responsive bandwidth of 15 GHz and recorded by a 2.5 GS/s real-time high-definition oscilloscope (TELEDY, HDO6104, 1-GHz bandwidth), allowing one to record time series up to 20 ms with a 400 ps/point resolution to obtain sufficient statistics. The recorded temporal traces of the filtered first to eighth-order Stokes lights and first to eighth-order anti-Stokes lights at the pump power of 810 mW are plotted in the right panel of Figs. 5(a) and 5(b), respectively. In the measured temporal traces of either Stokes light or anti-Stokes light, the intensity fluctuations of the time trace become more significant, and the occurrence of extreme events becomes more frequent as the Stoke/anti-Stokes order increases. This is mainly because the noises and instabilities induced by the intrinsic noise-seeded SBS process, the random mode resonance, as well as other noise sources are introduced in each low-order
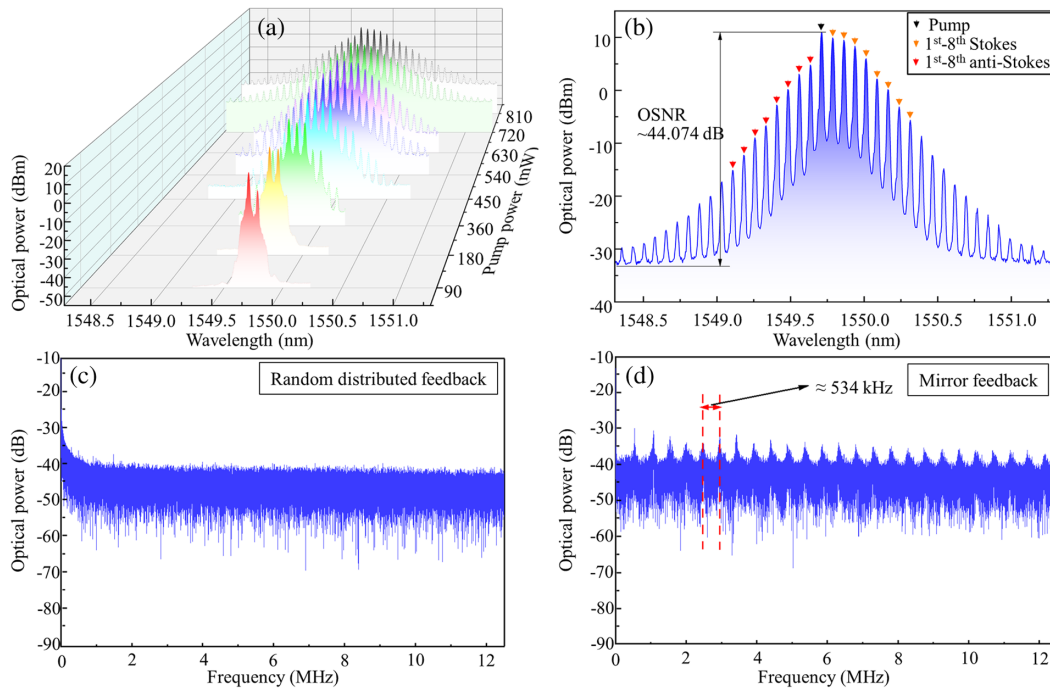
Fig. 4 Measured optical spectrum of the BRFLC output (a) at different pump powers and (b) at a pump power of 810 mW with 21 orders of Stokes lights and 18 orders of anti-Stokes lights; power spectra of the first-order Stokes lights of the Brillouin fiber laser comb with (c) random distributed feedback and (d) mirror feedback.
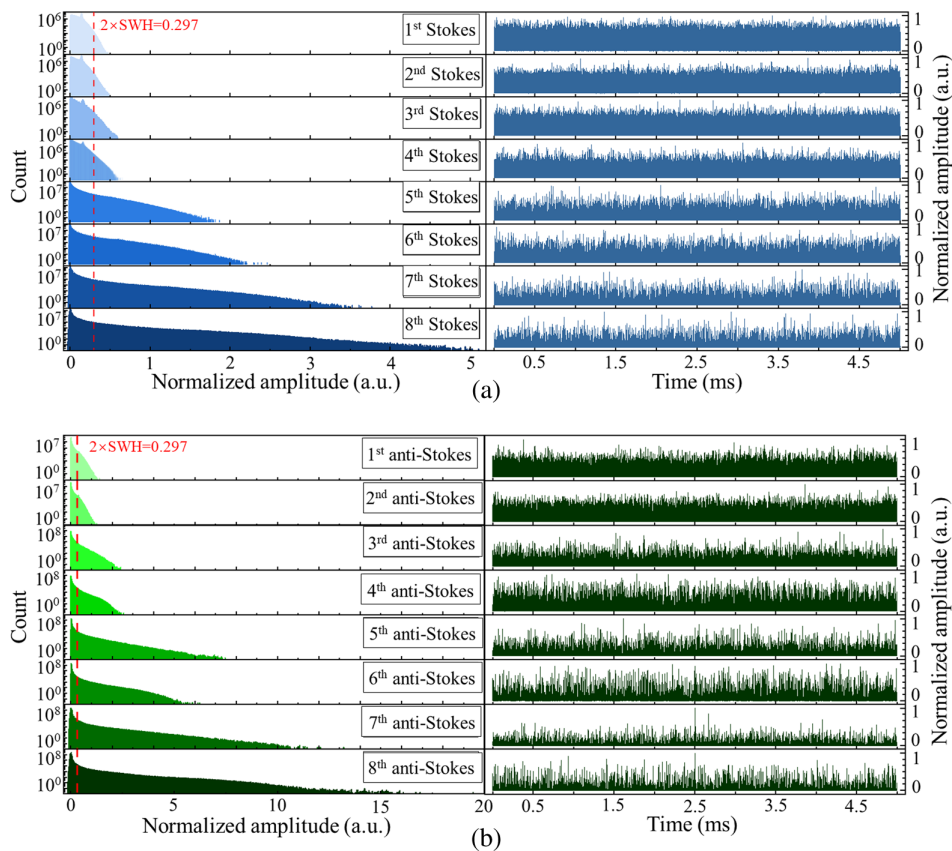

Fig. 5 Statistical histograms (left panel) of the pulse amplitudes in typical temporal traces (right panel) of first- to eighth-order (a) Stokes and (b) anti-Stokes lights at the pump power of 810 mW. The red dashed lines mark the 2×SWH.

Stoke/anti-Stokes light, which is then gradually transferred and accumulated to higher-order Stokes/anti-Stokes light through the cascaded SBS process and the quasi-phase-matched FWM process, making the higher-order Stokes/anti-Stokes light accumulate a larger amount of noise. These accumulated noises are then exponentially amplified by the MI process, which interacts with the cascaded SBS, the quasi-phase-matched FWM, as well as the random mode resonance process, and thus exhibit more severe instabilities in the output.

To characterize the statistical properties of the temporal traces of the Stokes/anti-Stokes lights, the statistical distribution of mutually normalized amplitudes of a total of 15 sets of temporal traces for each-order Stokes/anti-Stokes light is given and shown in the left panel of Figs. 5(a) and 5(b). In the statistical distribution, the red vertical dashed line marks the amplitude value twice the significant wave height (SWH), which is defined as the mean height of the highest third of events. The intensity fluctuation events with amplitude greater than 2×SWH are considered as optical RWs.[47] From the long-tailed and highly skewed statistical intensity distribution in Fig. 5, optical RW behavior is confirmed in all the Stokes and anti-Stokes lights

under study, and the occurrence probability of these extreme events increases with the order. The tails of the histogram become progressively longer as the order increases, reflecting the reduced stability and the gradually increasing maximum amplitude of the optical RWs in the temporal output. Compared with the typical Gaussian-shaped statistical distribution for standard stabilized continuous laser output, the exponential distribution appearing here is caused by the intense unstable temporal modulation resulting from the noise-driven MI that interacts with the cascaded SBS, the quasi-phase-matched FWM, as well as the random mode resonance process.

The statistical results of the temporal output traces of the Stokes/anti-Stokes lights in the BRFLC as a function of the Stokes/anti-Stokes order and pump power are illustrated in Fig. 6. Note that some spectral components of high-order Stokes/anti-Stokes lights that can be observed in the optical spectra as shown in Fig. 4(a) are not included here due to the failure of lasing resonance for these Stokes/anti-Stokes lights because of insufficient nonlinear optical gain. As shown in Fig. 6(a), the first- to third-order Stokes lights exhibit optical RW behavior with an extremely low and near-zero probability
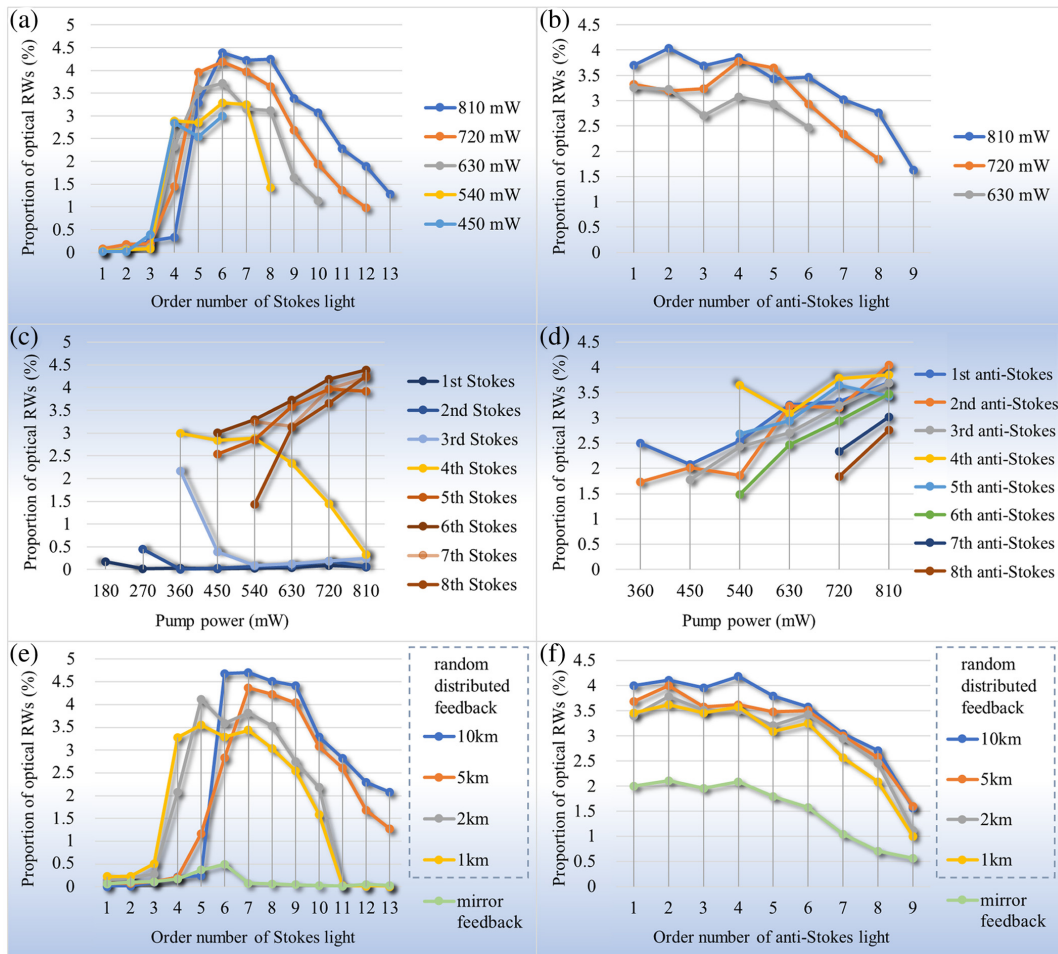
Fig. 6 Evolution of the proportion of optical RWs as a function of (a) the Stokes and (b) anti-Stokes order, and as a function of pump power for (c) Stokes and (d) anti-Stokes lights of different orders; evolution of the proportion of optical RWs as a function of (e) Stokes and (f) anti-Stokes order for cases of random distributed feedback provided by RSFs of different lengths and mirror feedback (green line), respectively.

regardless of the condition with high pump power. This is mainly attributed to the highly efficient SBS process with sufficient Brillouin gain and low cumulative noise for the generated low-order Stokes lights, which results in a stable random laser output with high coherence. Note that for the generation and amplification of the Stokes lights of the first three orders, the cascaded SBS process plays a dominant role owing to the sufficiently high Brillouin gain for low-order Stokes lights in the complex nonlinear interactions, though the quasi-phase-matched FWM process is also triggered and involved. Although noise transfer and additional noises from random mode resonances do occur in the generation of higher-order Stokes light from lower-order Stokes light, which may lead to an increase in the optical RW ratio of higher-order Stokes lights, the resonant SBS process in the BRFLC would increase the efficiency of the cascaded SBS as the pump power increases, which can suppress the noise generation and transfer through highly coherent random mode resonances in the laser cavity, thus preventing the intensified unstable temporal modulation induced by the MI process, ultimately maintaining the occurrence probability of optical RWs at a stable low level. For the fourth- to sixth-order Stokes light, the proportion of the optical RWs is observed to increase with the order. This is because, for the generation and amplification of the Stokes lights of fourth order and above, the FWM process is enhanced with a higher parametric gain coefficient and starts to interact with the cascaded SBS process, which at the same time starts to decay due to the more significate pump depletion effect as the order increases. As a result, the FWM process starts to play a more significant role than the cascaded SBS process in generating and amplifying these high-order Stokes lights. Large amount of extra noise would be introduced to the higher-order Stokes lights and anti-Stokes lights due to the susceptibility of the quasi-phase-matched FWM process to the random mode resonance and noise perturbations from the external environment. These noises are significantly amplified by the noise-driven MI and exert unstable temporal modulation on the resonant Stokes/anti-Stokes lights, thus elevating the emergence probability of optical RWs behavior. For Stokes lights of sixth order and above, the proportion of RW behavior shows a decreasing trend as the order increases. This is due to the fact that the cascaded SBS process becomes less efficient for higher-order Stokes lights as the more severe pump dissipation in the SBS process makes the power of Stokes lights at a low level, thus suppressing the efficiency of the quasi-phase-matched FWM process among these Stokes lights, as well as the nonlinear interaction with the cascaded SBS process, and finally reducing the occurrence chance of extreme events. In Fig. 6(b), the proportion of optical RWs in anti-Stokes lights decreases with the order at different pump powers. This could be understood by the fact that the FWM process plays a major role in the generation of anti-Stokes lines, so the mechanism accounting for the variation of optical RWs' proportion in anti-Stokes lines as a function of the anti-Stokes order is similar to that for higher-order Stokes lines (above the sixth order). Moreover, it is noteworthy that the proportion of RWs in anti-Stokes light is generally higher than that in Stokes light, which is mainly due to stronger instabilities introduced during the quasi-phase-matched-FWM-dominated nonlinear interactions.

In addition, the influence of the pump power on the proportion of RWs appearing in Stokes and anti-Stokes lights of different orders was carefully explored; the statistical results are shown in Figs. 6(c) and 6(d), respectively. In Fig. 6(c), three different trends are observed for the first eight orders of Stokes lights under investigation. As the pump power increases, the proportion of RWs appearing in the higher-order (fifth- to eighth-order) Stokes lights increases almost monotonically, which is mainly due to the high pump power-induced enhanced efficiency of the nonlinear interactions, including the cascaded SBS and quasi-phase-matching FWM process. For the lower-order (first- to third-order) Stokes lights, a low proportion of RWs is exhibited and maintained over the pump power variation range, and this proportion also shows a significant decreasing trend with the increase of the pump power below ∼550 mW. The reason for this is that for the low-order Stokes lights, the increase in the pump power would enhance the efficiency of the cascaded SBS effect that dominates the generation of low-order Stokes lights and enables the generated Stokes lights to resonate efficiently in the laser cavity, thus suppressing noise generation and transfer and improving the lasing output stability with fewer optical RWs to emerge. In fact, when the pump power increases to about 360 mW, at which the third-order and fourth-order Stokes lights are generated, the pump depletion effect weakens the cascaded SBS process for high-order Stokes lights and gives way to the FWM process, which gradually dominates the generation process of the fourth-order Stokes light. Therefore, in this critical state, the quasi-phase-matched FWM process induces noises with the assistance of the random mode resonance and the external noise perturbations. These noises are then amplified by the noise-induced MI process and impose the unstable temporal modulation on the generated fourth-order Stokes light, making the output of the fourth-order Stokes light exhibit a higher proportion of optical RWs. But as the pump power increases, the cascaded SBS process gradually re-dominates the generation process of the fourth-order Stokes light, which enhances the resonant cascaded SBS process and reduces the proportion of RWs. In Fig. 6(d), with the increase of the pump power, the proportion of RWs in all anti-Stokes lights shows an obvious upward trend and higher values than those of the high-order Stokes lights. This is mainly due to the fact that the cascaded SBS process contributes little gain to the generation and amplification of the anti-Stokes lights, which are otherwise mainly attributed to the parametric gain provided by the FWM process. As a result, anti-Stokes lights suffer from strong instabilities and thus exhibit a high proportion of RWs due to the quasi-phase-matched FWM process. Moreover, the power of all the Stokes and anti-Stokes lights that participated in the FWM process increases with the pump power, which in turn enhances the efficiency of the quasi-phase-matched FWM to generate and amplify the anti-Stokes lights. In this case, more noise is introduced by the quasi-phase-matched FWM, which is amplified by the MI process and thus imposes intensified unstable temporal modulation on the anti-Stokes light, resulting in a significant increase in the proportion of RWs appearing in the anti-Stokes light output.

The influence of the RSF length on the optical RWs' behavior is also investigated experimentally. It is worth noting that when the length of the RSF is altered, the strength of the feedback provided by the RSF would vary accordingly, resulting in different lasing states if the pump power is fixed at the same level. To have a fair comparison for cases with different lengths of RSF, the pump power in the BRFLC is finely controlled to make sure that the generated Stokes/anti-Stokes lights are of almost the same power level for all cases. Then the proportion of RWs appearing in Stokes and anti-Stokes lights for BRFLC employing RSFs with different lengths was explored; the results

are shown in Figs. 6(e) and 6(f). It is found that the proportion of optical RWs in most of the Stokes/anti-Stokes lights is increased when the RSF length increases. The reason for this phenomenon is that the length of the main cavity of the BRFLC is extended when longer RSF is utilized, which allows more densely distributed random modes to be involved in the random mode resonance process, thus enhancing the instabilities induced by mode hopping and multimode resonance interacting with the cascaded SBS process, the quasi-phase-matched FWM process, as well as the noise-driven modulation instability process. It is also noted that for low-order (below the sixth-order) Stokes lights, the proportion of RWs shows a decreasing trend with the increase in the RSF length. This is probably attributed to the more efficient cascaded SBS process with enhanced feedback from RSF with increased length for low-order Stokes lights, since the cascaded SBS process plays a dominant role in the complex nonlinear interactions owing to the sufficiently high Brillouin gain for low-order Stokes lights. As a result, this leads to a stabler random laser output with lower cumulative noise and higher coherence in the output of low-order Stokes lights. In addition, the RSF is replaced by an FM that is connected after point A in Fig. 1 to compare optical RWs' behaviors associated with fixed-point reflection feedback and random distributed feedback. The evolutions of the proportion of the optical RWs as a function of the Stokes/anti-Stokes order in the Brillouin fiber laser comb with the mirror feedback are illustrated by the green line in Figs. 6(e) and 6(f), which exhibit a distinct trend compared with the case of random distributed feedback. In Fig. 6(e), the proportion of the optical RWs in Stokes lights is maintained at a low level, which is mainly because in the case of mirror feedback, the density of the longitudinal modes in the resonant cavity is reduced and the mode intervals are no longer random compared to the cases of random distributed feedback, resulting in effective suppression of the instabilities induced by the mode hopping and multimode resonance and thus inhibiting the emergence of optical RWs. In Fig. 6(f), the evolutions of the proportion of the optical RWs of anti-Stokes lights in the case of random distributed feedback and mirror feedback exhibit similar trends. However, the proportion of optical RWs in anti-Stokes lights of different orders in the mirror feedback case is lower than that in the random distributed feedback case. On the one hand, this is due to the fact that the absence of dense random modes in the mirror feedback case allows the alleviation of the instability induced by the random mode resonance and its interactions with the nonlinear optical processes. On the other hand, a stabler laser resonance is established in the case of mirror feedback, which allows less noise to be accumulated and transferred during the cascaded SBS process, and the FWM process to deteriorate the stability of the resonant Stokes/anti-Stokes lights. In addition, a higher proportion of the optical RWs in anti-Stokes lights is observed compared with that in the Stokes lights in the case of mirror feedback. This is mainly caused by the partial random mode resonance with the random distributed feedback provided by the Rayleigh scattering in HNLF for the anti-Stokes lights, which would introduce perturbations to deteriorate the stability of the resonant anti-Stokes lights. Although the FM would also provide fixed-point feedback for anti-Stokes lights circulating inside the cavity, the so-called partial random laser resonance plays a more dominant role in the clockwise-propagating anti-Stokes lights than the mirror feedback from the FM, as the clockwise-propagating anti-Stokes lights are mainly amplified

by the FWM process in the HNLF, for which the cascaded SBS process contributes little gain for the anti-Stokes lights. As a result, the nonnegligible proportions of RWs in the anti-Stokes lights can be observed. For resonant Stokes light in the case of mirror feedback, though Rayleigh scattering in the HNLF would also contribute random distributed feedback during the lasing resonance, the mirror feedback provided by the FM is the dominant one that contributes to a relatively stabilized lasing resonances for the Stokes lights.

The temporal trace of the fourth-order Stokes light output is recorded and illustrated as an example shown in Fig. 7(a), with a local close-up view given in Fig. 7(b). Clear pulse-like intensity fluctuations with different intervals, durations, and amplitudes can be seen, which are mainly induced by the noise-driven MI that interacts with the cascaded SBS, the quasi-phase-matching FWM process, and the random mode resonance process. The pulse marked with a red dashed box in Fig. 7(b) is a typical temporally localized optical RW generated in the BRFLC, with an amplitude about 2 to 25 times higher than that of the surrounding regular pulses. In Fig. 7(c), a temporal trace of the second-order Stokes light in a time span of 5 ms is divided into 10,000 500-ns-long segments, which are then reorganized as a two-dimensional (2D) image. Two typical optical RW events are observed, with one marked with orange dashed ellipses in the figure that shows a single peak with bright color (RW1), and the other one marked with red dashed boxes showing special intensity distribution (RW2). The pulse shapes of the two kinds of RWs are given in the inset of Fig. 7(c), where RW1 shows a normal RW pulse shape and RW2 is a frequently encountered special RW with chair-like pulse shape, i.e., a sharp leading edge followed by a trailing plateau. The generation of these chair-like pulses is mainly attributed to the transient effect of the SBS process.[48] When the transient power within the leading part of the Gaussian-like RW pulse is higher than the SBS threshold of the Brillouin gain fiber, the transient SBS process would be triggered, and the power of the RW pulse is significantly depleted in a very short time. When the transient SBS takes place, power depletion would be induced in the Gaussian-like pulse right after the point of the pulse duration where the transient pulse power surpasses the SBS threshold. As the transient SBS proceeds, the power of the RW pulse is rapidly reduced to a level lower than the threshold of the transient SBS, stopping the SBS process. The power of the trailing part of the pulse is no longer reduced and remains at a relatively constant power level until the rear edge of the RW pulse owing to the failure of triggering the SBS process. Note that the RW pulse not only acts as the pump that transfers energy to the neighboring higher-order Stokes light through the SBS process, but also obtains energy from the neighboring lower-order Stokes light through the cascaded SBS process. In the latter process, since the RW pulse is mainly built up in the backward direction with respect to the pump light (or neighboring lower-order Stokes light), in which the front edge of the RW pulse experiences the highest transient Brillouin gain, the leading edge of the RW pulse becomes sharper with the enhanced SBS process by increasing the pump power.

In the statistical analysis of the laser output for multi-order Stokes and anti-Stokes lights in the BRFLC, it is found that there is a peak region in which the counting numbers for a certain output temporal amplitude range are significantly higher than those of neighboring regions, as shown in Fig. 5. To analyze this phenomenon in more detail, statistical histograms of
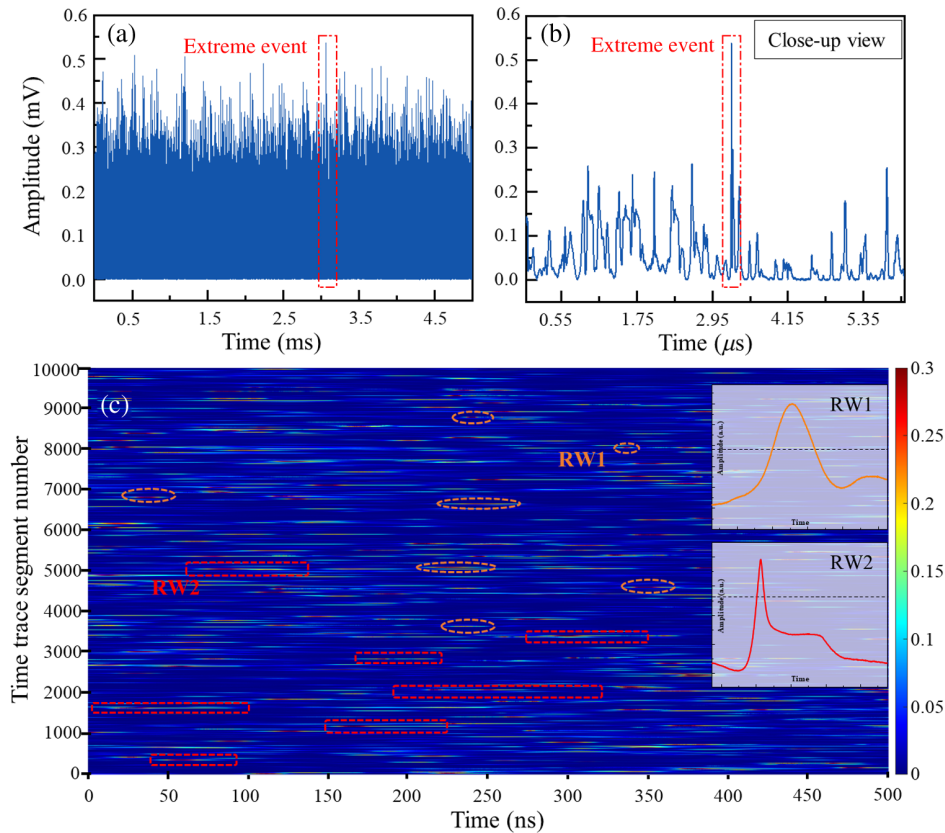
Fig. 7 (a) Temporal trace of the fourth-order Stokes light in a time span of 5 ms; (b) close-up view of the temporal trace in a time span of 6 μs; (c) evolution of consecutive temporal traces around temporally localized optical RW events of the second-order Stokes light at a pump power of 810 mW; inset, typical pulse shapes of the RW1 and RW2. The black dashed lines mark the 2×SWH.

the output amplitude with linear and logarithmic count scales are given in Fig. 8 for the first- to fourth-order Stokes lights and first- to second-order anti-Stokes lights. As shown in Figs. 8(a)–8(d), the amplitude histogram with the linear scale exhibits a higher counting number around the normalized amplitude of ~0.145, which is in agreement with the trailing plateau of the chair-like pulses and thus confirms the presence of frequently emerged temporally localized structures in the temporal traces, i.e., RW2 plotted in Fig. 7(c). A red dashed line marking the amplitude value that is twice the SWH value and a black dashed line marking the trailing plateau amplitude of the chair-like pulse are plotted in Fig. 8. It is clearly seen that most of the amplitude distribution along the pulse profile does not exceed the optical RW threshold for the given Stokes light. As the Stokes order increases, the count number for low temporal output amplitude values ($< \sim 0.1$) gradually increases, while the count number for the observed temporally localized structures gradually decreases. The main reason for this is that as the Stokes order increases, the cascaded SBS effect becomes progressively weaker and provides reduced Brillouin gain due to the pump depletion effect, which leads to the reduced number of resonant random modes in the main cavity with decreased coherence, thus highlighting the L-shaped amplitude distribution caused by the noise-driven MI and its interaction with the less efficient cascaded SBS, the quasi-phase-matched FWM, and the random mode resonance process. It is worth noting that the gap

between the count peak for the observed amplitude of the temporally localized structures and the double SWH becomes gradually smaller as the Stokes order increases, which is owing to the increased occurrence probability of the optical RWs for the high-order Stokes light due to the enhanced MI with the accumulation of noises. Since the anti-Stokes lights are generated and amplified almost exclusively through the quasi-phase-matched FWM process, their statistical histograms of output amplitude exhibit a more distinct L-shaped distribution with long tails, as shown in Figs. 8(e) and 8(f). From the insets in Figs. 8(e) and 8(f), small peak regions with counting numbers for a certain output temporal amplitude range higher than those of neighboring regions are still observed in the anti-Stokes light, with most of the amplitude distribution along the pulse profile exceeding twice the SWH, which indicates that the chair-like pulses generated in the temporal output can be grouped as optical RWs, both for its sharp leading edge and the following trailing plateau. The explanation for this phenomenon is that the quasi-phase-matched FWM process and the less efficient cascaded SBS process among the anti-Stokes lights introduce heavy noise, which is then intensified by the MI process, imposing the stronger unstable temporal modulation on the anti-Stokes lights, and triggering the more frequent occurrence of optical RWs with extreme amplitudes.

In addition to the analysis of the statistical evolution of the RWs' behavior, investigations on the pulse properties of the
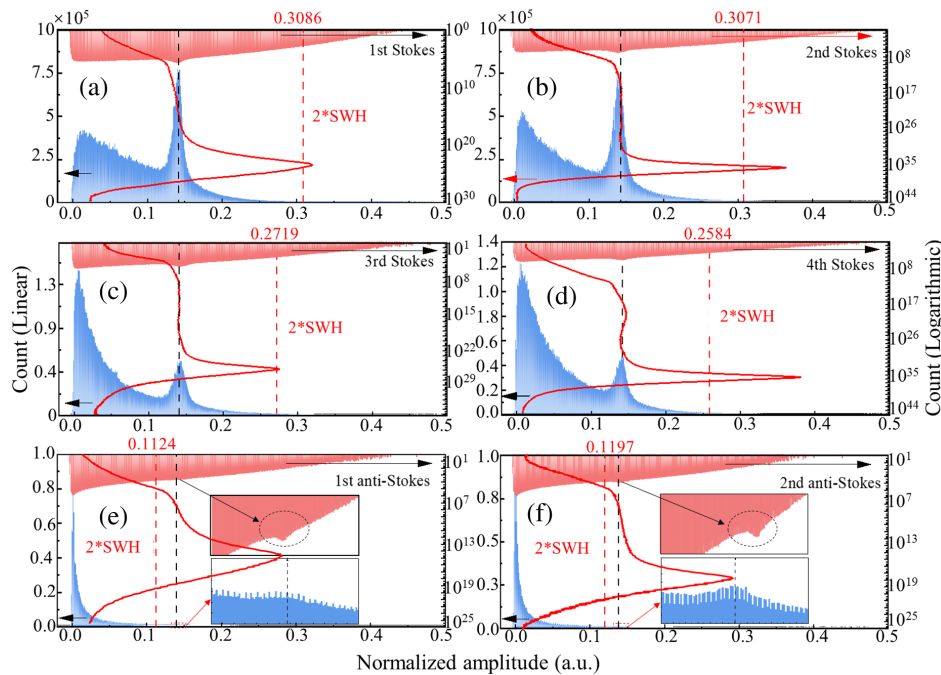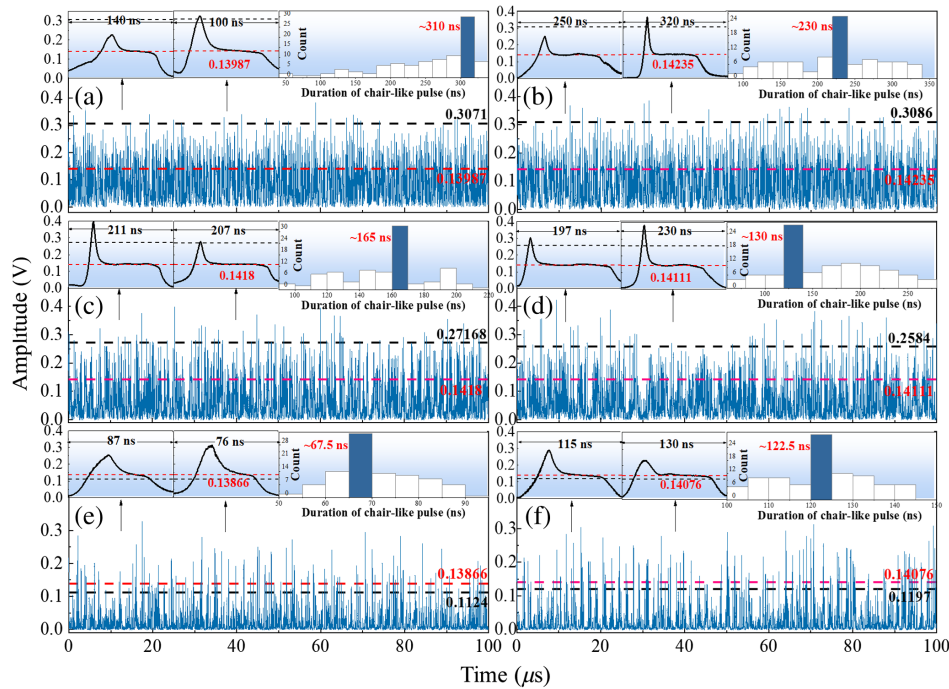
Fig. 8 Statistical histograms of output amplitude of (a) the first-order Stokes, (b) second-order Stokes, (c) third-order Stokes, (d) fourth-order Stokes, (e) first-order anti-Stokes, and (f) second-order anti-Stokes lights with linear (blue) and logarithmic (red) count scale. The red and black dashed vertical lines mark the 2×SWH and the amplitude of the counting peak, respectively.

temporally localized RW structures are particularly important. A detailed illustration of the observed temporally localized structures with chair-like pulse shape and high occurrence frequency is presented in Fig. 9, with pulse examples extracted from the output temporal traces from the first- to fourth-order Stokes lights and first- and second-order anti-Stokes lights. As shown in the left insets of Figs. 9(a)–9(f), chair-like pulses are observed in the time traces of Stokes/anti-Stokes lights. This chair-like pulse consists of a sharp leading edge and a trailing plateau region, and the amplitudes along its plateau region are exactly located within the amplitude peak region of the statistical histograms in Fig. 8. By comparison, it can be found that the spike width of the chair-like pulses in the Stokes lights is relatively narrow and the duration of its plateau region is relatively long, while the spike width in the anti-Stokes lights becomes larger and the duration of its plateau region is maintained at a short level. In the experiment, durations of 100 chair-like pulses in the temporal traces of each Stokes/anti-Stokes light are measured and statistically analyzed. The statistical distributions of the durations of chair-like pulses that emerged in the selected Stokes/anti-Stokes lights are shown in the right insets of Figs. 9(a)–9(f). Durations of these chair-like pulses show a general trend to decrease as the Stokes order increases while they increase as the anti-Stokes order increases. The possible reason for this evolutionary trend is the order-by-order pulse compression effect for the Stokes/anti-Stokes lights in the cascaded SBS process. In addition, the duration of the chair-like pulses appearing in the anti-Stokes lights is significantly shorter than that in the Stokes lights. This is mainly due to the fact that most of the pulses in anti-Stokes lights are generated by the FWM process with a high parametric gain coefficient occurring within the short high-peak-power duration of Stokes pulses of different

orders. It is worth mentioning that most of the amplitude distribution along the chair-like pulse profile in the Stokes light output does not exceed the optical RW threshold, and the opposite situation occurs for the anti-Stokes light output in Fig. 9, showing a good match with the results in Fig. 8.

To further investigate the pulse shape evolution of the temporally localized chair-like RWs with Stokes/anti-Stokes orders, chair-like RW pulses from the first to third order and the sixth-order Stokes lights and the second-order anti-Stokes lights are given in Fig. 10 for comparison. In the plot, the black dashed line marks the amplitude value that is twice the SWH value and the red dashed line marks the trailing plateau amplitude of the chair-like pulse. In Figs. 10(a)–10(c), it can be found that the optical RWs which frequently appear in the first- to third-order Stokes light exhibit a similar chair-like pulse shape, with a sharp leading edge followed by a trailing plateau. But the optical RWs appearing in the sixth-order Stokes light and the second-order anti-Stokes light as shown in Figs. 10(d) and 10(e) exhibit irregular pulse shapes and extremely high peaks, well above the RW threshold. This behavior is mainly attributed to the fact that the dominant nonlinear process evolves from the cascaded SBS process for the generation of the first- to third-order Stokes lights to the FWM process for the generation of the sixth-order Stokes and second-order anti-Stokes lights. Thus, the intensified noises by the MI process are introduced to high-order Stokes lights and anti-Stokes lights, leading to pulse splitting in the originally chair-like-pulse-shaped RWs, thus generating large numbers of RWs with irregular pulse shapes with even more extreme peak amplitudes.

To investigate the pulse shape evolution of the temporally localized chair-like RWs with the pump power, typical RW pulses in the time traces of the first-order to fourth-order

Fig. 9 Temporal traces, typical pulse shape, and statistical distribution of duration of chair-like pulses in the output of (a) first-order Stokes, (b) second-order Stokes, (c) third-order Stokes, (d) fourth-order Stokes, (e) first-order anti-Stokes, and (f) second-order anti-Stokes lights at a pump power of 810 mW. The red and black dashed lines mark the amplitude of the trailing plateau of the chair-like pulse and the 2×SWH, respectively.
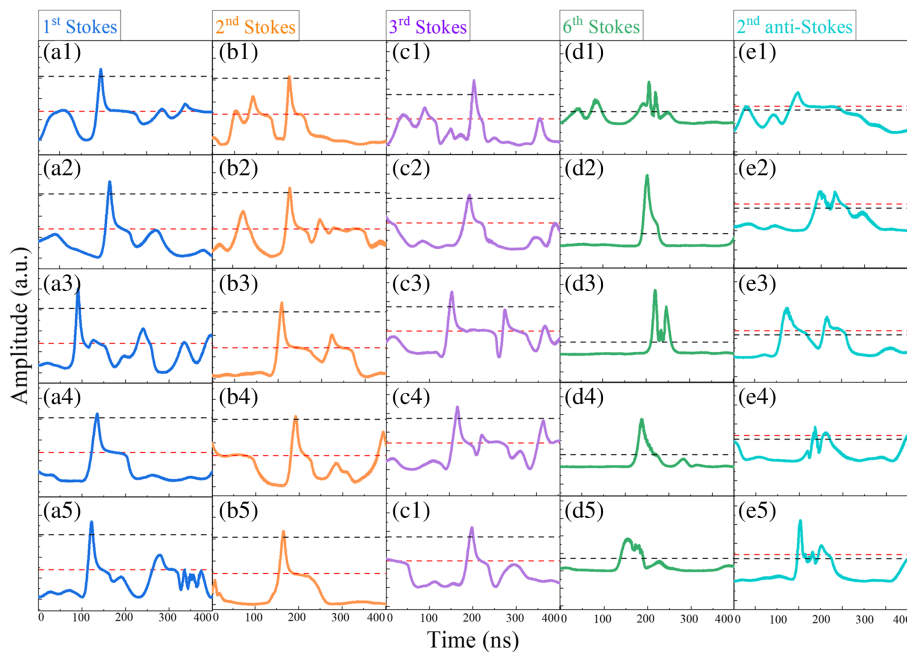
Fig. 10 Pulse shapes of the temporally localized optical RWs appearing in (a1–a5) the first-order Stokes, (b1–b5) second-order Stokes, (c1–c5) third-order Stokes, (d1–d5) sixth-order Stokes, and (e1–e5) second-order anti-Stokes lights. The black and red dashed lines mark the 2×SWH and the amplitude of the trailing plateau of the chair-like pulse, respectively.
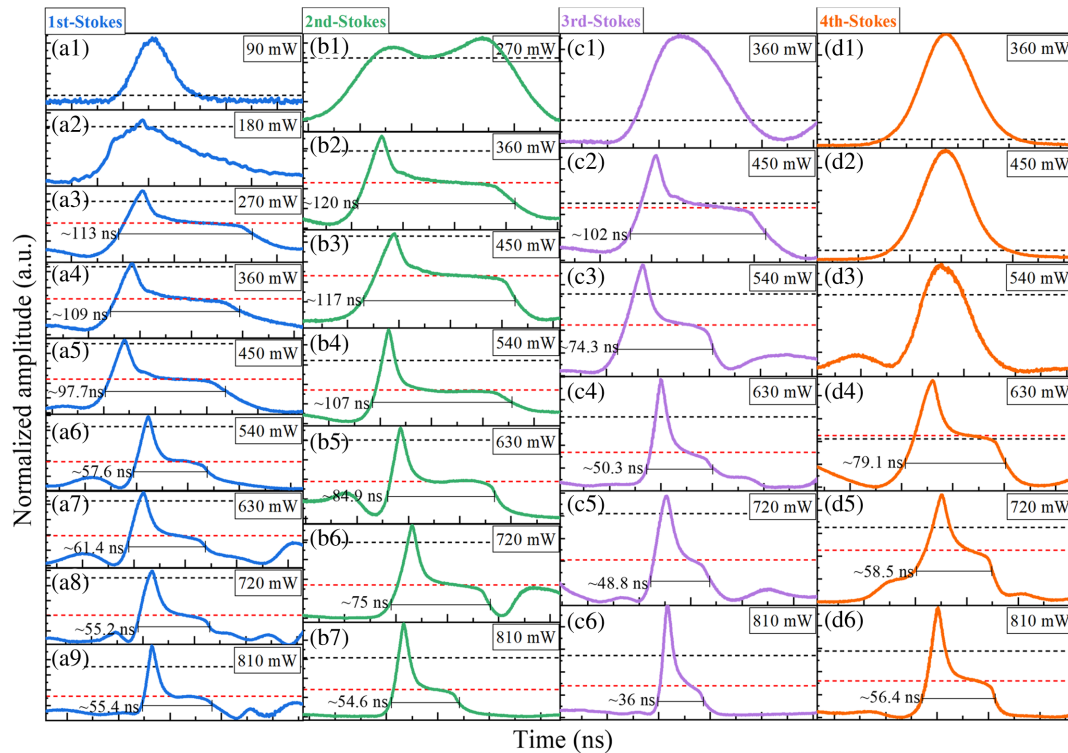
Fig. 11 Duration manipulation for temporally localized optical RWs in (a1–a9) the first-order Stokes, (b1–b7) second-order Stokes, (c1–c6) third-order Stokes, and (d1–d6) fourth-order Stokes lights realized by adjusting the pumping power. The black and red dashed lines mark the 2×SWH and the amplitude of the trailing plateau of the chair-like pulse, respectively.

Stokes lights at different pumping powers are given in Fig. 11, respectively. In Figs. 11(a1)–11(d1), pulse shapes of the optical RWs generated in the Stokes lights are either Gaussian-like or amorphous when the pump power is at relatively low levels. With the increase of pump power, the chair-like RW pulses appear and gradually become universal in the temporal output, and the duration of most RWs progressively becomes shorter, as shown by the rest of the plots in Fig. 11, which indicates that the pulse duration of optical RWs can be manipulated by controlling the pump power. It is worth noting that as the Stokes order increases, higher pump power is required to convert the amorphously shaped RW pulse to a standard chair-like RW pulse.

It is intriguing that the above experimental results and analysis have revealed the potential for manipulating optical RWs in the BRFLC system. The occurrence probability of RWs in each-order Stokes/anti-Stokes light can be effectively tuned by adjusting the pump power. This probability also shows a certain evolution with the order of Stokes/anti-Stokes lights, which provides the opportunity for manipulating and studying optical RWs by selecting Stokes/anti-Stokes lights of different orders through optical filtering. For Stokes lights of different orders, the initially emerged amorphous RW pulse can be converted into a standard chair-like pulse when the pump power reaches a certain threshold. The duration and amplitude of the chair-like pulse can also be adjusted by controlling the pump light power above the conversion threshold. These studies provide a promising way for either controlling or harnessing the optical RWs occurring in laser systems. Furthermore, the characteristics

of the noise-driven MI, the cascaded SBS, and the quasi-phase-matched FWM process, including their dependence on dispersion, polarization, wavelength, and pump power, can be exploited to further modulate the RW properties in a complex nonlinear optical system. Importantly, the studies of the extreme amplitude RWs exhibit promising potentials to be harnessed for the generation and investigation of high-power optical pulses, extreme solitons, and other rare events in optical laser systems.

4 Conclusion

The extreme event of optical RWs with temporally localized structures is observed in the BRFLC. The emergence of the optical RW is attributed to the noise-driven MI that interacts with the cascaded SBS, the quasi-phase-matched FWM, and the random mode resonance process in the BRFLC. Experiments are performed to investigate the temporal and statistical characteristics of the BRFLC output, unveiling the emergence and evolution rules of the observed optical RWs' behavior. Meanwhile, temporally localized structures including chair-like pulse with a sharp leading edge followed by a trailing plateau appear frequently in the output of BRFLC, which can evolve to chair-like RW pulses with adjustable pulse duration and amplitude under controlled conditions. This investigation unveils the optical RW behavior in BRFLC and paves the way for RW prediction, manipulation, and inhibition. Future studies are necessary to investigate the generation and evolution of chair-like RW pulses in the BRFLC through theoretical modeling and simulation.

Disclosures

The authors declare that they have no competing interests.

Code and Data Availability

Data underlying the results presented in this paper are not publicly available at this time but may be obtained from the authors upon reasonable request.

Authors' Contributions

Acknowledgments

References

1. A. Chabchoub, N. P. Hoffmann, and N. Akhmediev, "Rogue wave observation in a water wave tank," *Phys. Rev. Lett.* **106**(20), 204502 (2011).
2. A. R. Osborne, M. Onorato, and M. Serio, "The nonlinear dynamics of rogue waves and holes in deep-water gravity wave trains," *Phys. Lett. A* **275**(5), 386–393 (2000).
3. D. R. Solli et al., "Optical rogue waves," *Nature* **450**(7172), 1054–1057 (2007).
4. X. Wei, Z. He, and W. Zhang, "Cascaded supercontinuum generation and rogue wave harnessing," *Chaos Solitons Fractals* **165**, 112858 (2022).
5. K. Hammani et al., "Optical rogue-wave-like extreme value fluctuations in fiber Raman amplifiers," *Opt. Express* **16**(21), 16467 (2008).
6. C. Bonatto, "Deterministic optical rogue waves," *Phys. Rev. Lett.* **107**(5), 053901 (2011).
7. M. G. Kovalsky, A. A. Hnilo, and J. R. Tredicce, "Extreme events in the Ti:sapphire laser," *Opt. Lett.* **36**(22), 4449 (2011).
8. C. Bonazzola et al., "Optical rogue waves in an all-solid-state laser with a saturable absorber: importance of the spatial effects," *J. Opt.* **15**(6), 064004 (2013).
9. S. Coulibaly et al., "Extreme events following bifurcation to spatiotemporal chaos in a spatially extended microcavity laser," *Phys. Rev. A* **95**(2), 023816 (2017).
10. R. Uppu and S. Mujumdar, "Physical manifestation of extreme events in random lasers," *Opt. Lett.* **40**(21), 5046 (2015).
11. K. Hammani, A. Picozzi, and C. Finot, "Extreme statistics in Raman fiber amplifiers: from analytical description to experiments," *Opt. Commun.* **284**(10), 2594–2603 (2011).
12. D. Majus et al., "Spatiotemporal rogue events in femtosecond filamentation," *Phys. Rev. A* **83**(2), 025802 (2011).
13. S. Randoux and P. Suret, "Experimental evidence of extreme value statistics in Raman fiber lasers," *Opt. Lett.* **37**(4), 500 (2012).
14. M. Luo et al., "Dissipative rogue waves generated by multi-soliton explosions in an ultrafast fiber laser," *Opt. Express* **30**(12), 22143 (2022).
15. J. Xu et al., "Optical rogue wave in random fiber laser," *Photonics Res.* **8**(1), 1 (2020).
16. R. Ma et al., "20 watt-level single transverse mode narrow linewidth and tunable random fiber laser at 1.5 μm band," *Opt. Express* **30**, 28795–28804 (2022).
17. L. Zhang et al., "Sub-kHz high-order mode Brillouin random fiber laser based on long-period fiber grating and distributed Rayleigh scattering in a half-open linear cavity," *Opt. Express* **31**(10), 15484–15494 (2023).
18. J. Ye et al., "Revealing the dynamics of intensity fluctuation transfer in random Raman fiber laser," *Photonics Res.* **10**, 618–627 (2022).
19. H. Wu et al., "Widely tunable continuous-wave visible and mid-infrared light generation based on a dual-wavelength switchable and tunable random Raman fiber laser," *Photonics Res.* **11**, 808–816 (2023).
20. P. Tovar, G. Temporão, and J. P. von der Weid, "Longitudinal mode dynamics in SOA-based random feedback fiber lasers," *Opt. Express* **27**(21), 31001–31012 (2019).
21. H. Wu et al., "1.5 μm low threshold, high efficiency random fiber laser with hybrid Erbium–Raman gain," *J. Lightwave Technol.* **36**(4), 844–849 (2018).
22. H. Zhang et al., "Quasi-kilowatt random fiber laser," *Opt. Lett.* **44**(11), 2613–2616 (2019).
23. Y. Zhang et al., "Tunable random Raman fiber laser at 1.7 μm region with high spectral purity," *Opt. Express* **27**(20), 28800–28807 (2019).
24. M. Pang, X. Bao, and L. Chen, "Observation of narrow linewidth spikes in the coherent Brillouin random fiber laser," *Opt. Lett.* **38**(11), 1866 (2013).
25. Y. Pang et al., "Single-longitudinal-mode short-cavity Brillouin random fiber laser via frequency auto-tracking with unpumped-EDF Sagnac loop," *Infrared Phys. Technol.* **127**, 104461 (2022).
26. L. Zhang et al., "Linearly polarized low-noise Brillouin random fiber laser," *Opt. Lett.* **42**(4), 739 (2017).
27. H. Wang et al., "Stabilizing Brillouin random laser with photon localization by feedback of distributed random fiber grating array," *Opt. Express* **30**(12), 20712 (2022).
28. Y. Xu et al., "Random Fabry–Perot resonator-based sub-kHz Brillouin fiber laser to improve spectral resolution in linewidth measurement," *Opt. Lett.* **40**(9), 1920–1923 (2015).
29. X. Feng et al., "Reconfigurable microwave photonic filter using multiwavelength erbium-doped fiber laser," *IEEE Photonics Technol. Lett.* **19**(17), 1334–1336 (2007).
30. D. Xiang et al., "Truly random bit generation based on a novel random Brillouin fiber laser," *Opt. Lett.* **40**(22), 5415 (2015).
31. H. Chen et al., "Advances in random fiber lasers and their sensing application," *Sensors* **20**(21), 6122 (2020).
32. H. Wu et al., "Temporal ghost imaging with random fiber lasers," *Opt. Express* **28**(7), 9957 (2020).
33. S. Gao et al., "High-speed random bit generation via Brillouin random fiber laser with non-uniform fibers," *IEEE Photonics Technol. Lett.* **29**(16), 1352–1355 (2017).
34. L. Zhang et al., "Multiwavelength coherent Brillouin random fiber laser with ultrahigh optical signal-to-noise ratio," *IEEE J. Sel. Top. Quantum Electron.* **24**(3), 1–8 (2018).
35. L. Zhang et al., "Multi-wavelength Brillouin random fiber laser via distributed feedback from a random fiber grating," *J. Lightwave Technol.* **36**(11), 2122–2128 (2018).
36. L. Zhang et al., "Linearly polarized multi-wavelength fiber laser comb via Brillouin random lasing oscillation," *IEEE Photonics Technol. Lett.* **30**(11), 1005–1008 (2018).

37. Y. Pang et al., "Frequency comb generation based on Brillouin random lasing oscillation and four-wave mixing assisted with nonlinear optical loop mirror," *Photonics* **10**(3), 296 (2023).

38. L. Talaverano et al., "Multiwavelength fiber laser sources with Bragg-grating sensor multiplexing capability," *J. Lightwave Technol.* **19**(4), 553–558 (2001).

39. S. Diaz, D. Leandro, and M. Lopez-Amo, "Stable multiwavelength Erbium fiber ring laser with optical feedback for remote sensing," *J. Lightwave Technol.* **33**(12), 2439–2444 (2015).

40. X. Wang et al., "Temporal optical rogue waves in high power short-cavity Yb-doped random fiber laser," *Opt. Laser Technol.* **149**, 107797 (2022).

41. R. W. Boyd, K. Rzaewski, and P. Narum, "Noise initiation of stimulated Brillouin scattering," *Phys. Rev. A* **42**(9), 5514–5521 (1990).

42. A. Yeniay, J.-M. Delavaux, and J. Toulouse, "Spontaneous and stimulated Brillouin scattering gain spectra in optical fibers," *J. Lightwave Technol.* **20**(8), 1425–1432 (2002).

43. X. M. Liu, "Broad and tunable multiwavelength fiber laser at the assistance of modulation-instability-assisted four-wave mixing," *Laser Phys.* **20**(4), 842–846 (2010).

44. G. A. Cranch and G. A. Miller, "Fundamental frequency noise properties of extended cavity erbium fiber lasers," *Opt. Lett.* **36**(6), 906 (2011).

45. S. Foster, "Fundamental limits on 1/f frequency noise in rareearth-metal-doped fiber lasers due to spontaneous emission," *Phys. Rev. A* **78**(1), 013820 (2008).

46. B. Saxena, "Noise characteristics for random fiber lasers with Rayleigh distributed feedback," Thesis, Université d'Ottawa/ University of Ottawa (2014).

47. P.-H. Hanzard et al., "Brillouin scattering-induced rogue waves in self-pulsing fiber lasers," *Sci. Rep.* **7**(1), 45868 (2017).

48. G. P. Agrawal, "Nonlinear fiber optics," in *Nonlinear Science at the Dawn of the 21st Century*, P. L. Christiansen, M. P. Sørensen, and A. C. Scott, Eds., pp. 195–211, Springer, Berlin, Heidelberg (2000).

Yuxi Pang received his BS degree from Shandong Jianzhu University in 2020, and his MS degree from Shandong University in 2023. He is currently working toward the PhD in optical engineering at the Center for Optics Research and Engineering and Key Laboratory of Laser and Infrared System of the Ministry of Education, Shandong University, China. His research interests include random fiber lasers, fiber lasers, and optical fiber sensing.

Yanping Xu received his BS degree in physics from Jilin University, China, in 2011, and his PhD in physics from the University of Ottawa, Canada, in 2017. Currently, he is a full professor at the Center for Optics Research and Engineering, Shandong University, China, and has been conferred the title of Taishan Young Scholar of Shandong Province and Qilu Young Scholar of Shandong University. From 2017 to 2018, he was at the Department of Physics, University of Ottawa, as a postdoctoral fellow. In 2018, he joined Ciena Corporation (originally known as Nortel Networks Corporation), Canada, as a fiber-optic communication research scientist. He has authored or co-authored more than 60 research papers in peer-reviewed journals and conference proceedings. His research interests include fiber-optic sensors, fiber lasers, random number generation, nonlinear fiber-optic effects, and fiber-optic communications. He has been invited to give oral presentations in OFS, OFC, CLEO, IEEE Sensors, and Photonics North conferences. He has served as a guest editor for *Sensors*, and as a reviewer for several peer-reviewed journals, including *Photonics Research*, *Optics Express*, *Optics Letters*, *IEEE Journal of Lightwave Technology*, *IEEE Photonics Technology Letters*, *IEEE Photonics Journal*, *Applied Optics*, *Optics Communications*, and *Optical Fiber Technology*.

Biographies of the other authors are not available.